Nano particle and defect detection: physical limit of state-of-the-art systems and novel measurement technique to improve upon this detection limit

Wouter D. Koek*, Erwin J. van Zwet, Hamed Sadeghian

TNO, Stieltjesweg 1, 2628CK, Delft, The Netherlands

ABSTRACT

Traditionally, (dark field) imaging based, particle detection systems rely on identifying a particle based on its irradiance. It can be shown that for a very smooth wafer with 0.1 nm surface roughness (rms) this approach results in a particle detection limit larger than 20 nm. By carefully studying the physical mechanism behind this practical limit, we have developed an alternative interferometric measurement technique that is able to improve upon this limit. This technique is based on the interferometric amplification of the particle signal, while choosing the phase of the reference beam carefully as not to amplify the coherent background speckle. Although this allows to detect particles that are 30% smaller, compared to irradiance based detection this technique poses much more stringent requirements on the wavefront errors of the imaging optics.

Keywords: particle detection, defect inspection, nanoparticle, interferometry, binary phase, surface roughness, difference detection

1. INTRODUCTION

Defects and particular contamination of wafers and masks has always been an issue in lithography systems. With the reduction in feature sizes over the years, preventing the presence of smaller particles and defects becomes increasingly relevant. Accordingly, the measurement tools that are used to characterize and qualify (unpatterned) wafers and masks must continuously improve upon the minimum detectable particle size. This particle-detection limit depends not only on the measurement concept and implementation, but also on the surface roughness of the substrate and the required detection statistics (e.g. allowed number of false positives), making it hard to unambiguously compare different specifications from different suppliers. Measurement tools that rely on irradiance-based detection are currently limited to the detection of particles (or other defects) of around 20 nm[1,2].

In this paper we report on the physical mechanism that drives this particle-detection limit. Based on this physical insight, we have developed an alternative measurement concept that is able to improve upon the detection limit by as much as 30%. In this paper we will present this new technique, and discuss its benefits, challenges and limitations.

2. TRADITIONAL PARTICLE DETECTION

In order to better appreciate the differentiating features of our new method, in this chapter we will first describe the particle detection limit, after which we will discuss and illustrate traditional irradiance-based dark-field particle-detection systems[1,3].

2.1 Particle detection limit

As long as a particle is very large (i.e. larger than the wavelength that is used to observe it), and the substrate on which it resides is very smooth (i.e. has a root mean square (rms) surface roughness that is much smaller than the wavelength used), the detection of such a particle presents little challenges. In such a case, if the substrate (with particle) is imaged in a dark field configuration, the particle will distinctively show up as a bright spot against an otherwise dark background[4].

*wouter.koek@tno.nl; phone +31-88-866-8002

However, as the particle becomes smaller, the amount of light scattered by it rapidly decreases (in the Rayleigh scattering regime the total scattered energy scales with the sixth power of the particle diameter)[5].

The incident light not only scatters from the particle, but also from the substrate (due to its inherent surface roughness). When (coherent) laser light is used, which is typically the case given the need for a high-brightness source, the surface-scattered light will generate a speckle pattern (i.e. a 'granular' pattern where the local irradiance can be many times the average irradiance)[6, 7].

When the particle becomes smaller, at some point the particle image's irradiance will become comparable to the average irradiance of the speckle background. Because both the particle image and the speckle size are determined by the numerical aperture of the imaging system, they will not only have similar irradiance but also have identical dimensions. Accordingly, the chance to mistakenly interpret a (bright) speckle as a particle, or vice versa, increases for decreasing particle sizes.

It is important to note that the requirements of a particle scanner typically allow for a very small number of false-positive measurements (i.e. report a particle when actually no particle is present). Because the statistics of a speckle pattern are well known[6, 7], it is possible to determine the probability if the brightest spot in a speckle image may simply be due to speckle statistics or should be considered a particle, thereby allowing for a statistical description of the false-positive probability.

To this end we define the peak-to-sigma ratio P as being the ratio of the peak irradiance in an image relative to the standard deviation of its irradiance. Figure 1 shows the number of false positives that can be expected for a system, that uses a wavelength of 193 nm and has a numerical aperture (NA) of approximately 0.5, when scanning a 150 mm × 150 mm area while using a certain peak-to-sigma criterion to identify a particle. The figure shows that, when using the same measurement system, smaller particles can be detected if more false-positives are allowed. As the false-positive rate is not always explicitly mentioned it is often hard to compare the particle-detection limit between different measurement tools. Internally we have defined an acceptable false-positive rate of 10. To allow for a sound comparison between various measurement concepts, for the remainder of this paper, we will thus require a peak-to-sigma ratio of 24 to be able to identify a particle with sufficient probability. In other words, if an image contains a bright spot where the irradiance exceeds the standard deviation of the irradiance in that image by a factor of 24 or more, it is determined that a particle must be present at that particular location.
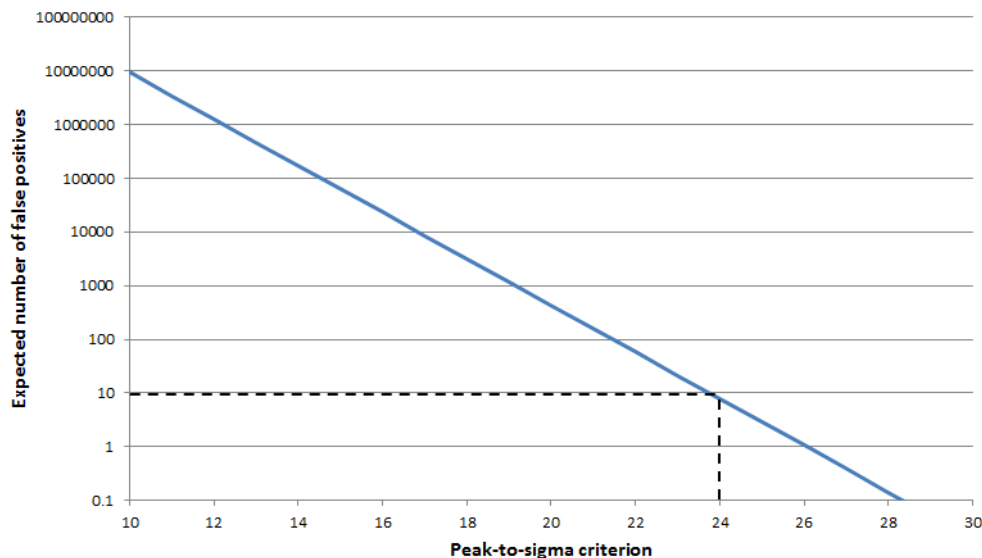

Figure 1. The number of false positives which can be expected when scanning a 150 mm × 150 mm area while using a certain peak-to-sigma criterion to identify a particle. This analysis is based on a particle scanner with λ = 193 nm and NA ≈ 0.5. In this study we allow for 10 false positives to occur when scanning a 150 mm × 150 mm area, and thus set the particle detection criterion at peak-to-sigma ratio $P \geq 24$.

2.2 Dark-field particle detection

Figure 2(a) shows a conceptual drawing of an off-axis illuminated dark field imaging system[1, 3]. By using an in-house developed numerical wavefront propagation code, based on Fourier optics[8], we have modelled the irradiance and phase distribution in the image plane. These simulations assume an illuminating wavelength of 193 nm, a numerical aperture of 0.5, unit magnification, and an rms surface roughness of 0.1 nm. Throughout our analyses we use numerically generated surfaces with a synthesized surface topology. Figure 3 shows the power spectral density of surface roughness as used throughout our simulations, and a comparison to actual wafer data[9].

Figure 2(b) shows the (peak-normalized) irradiance of the wavefront in the image plane, whereas Figure 2(c) shows its phase. It is important to note that the phase is more or less constant within a single speckle, but has uniformly distributed random values over the various speckles. Figure 4 helps to explain this random phase behavior.

Figure 4(a)-(d) show various components of the wavefront around the substrate, where the red, green and blue arrows represent the local wavefront in phasor notation (i.e. the length of the vector represents the absolute value of the local complex amplitude of a wavefront, and the orientation of the vector represents the phase of the local wavefront). Figure 4(a) shows that for an off-axis illumination beam there is a linear gradient in the phase of the wavefront falling onto, and thus reflecting from, a perfectly flat surface. It is important to realize that the red phasors represent the specular reflection which, based on the definition of dark-field imaging, will not contribute to the image (it's frequency content is fully blocked by the aperture of the imaging system).

However, as Figure 4(b) illustrates, the situation is different for a rough surface. The reflected (or secondary) wave, i.e. the green phasors, originating from a region that is elevated with respect to the average surface height will be slightly advanced relative to the specular reflected wave. Likewise, the secondary wave emanating from a 'low' region of the surface will be somewhat delayed.
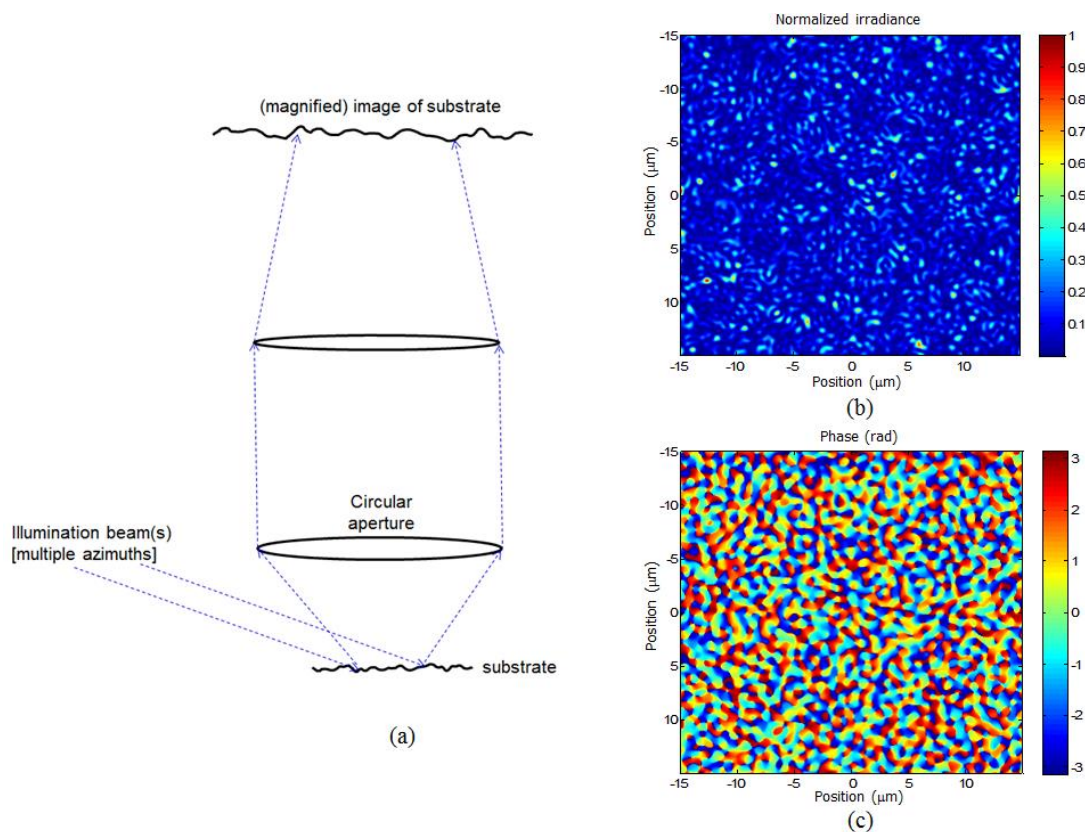

Figure 2. (a) Conceptual drawing of an off-axis dark-field particle-detection system (here shown without a particle on the substrate). In order to suppress speckle the sample may be illuminated under multiple azimuths[1]. (b) Typical example of the irradiance in the image plane, and (c) the phase in the image plane.
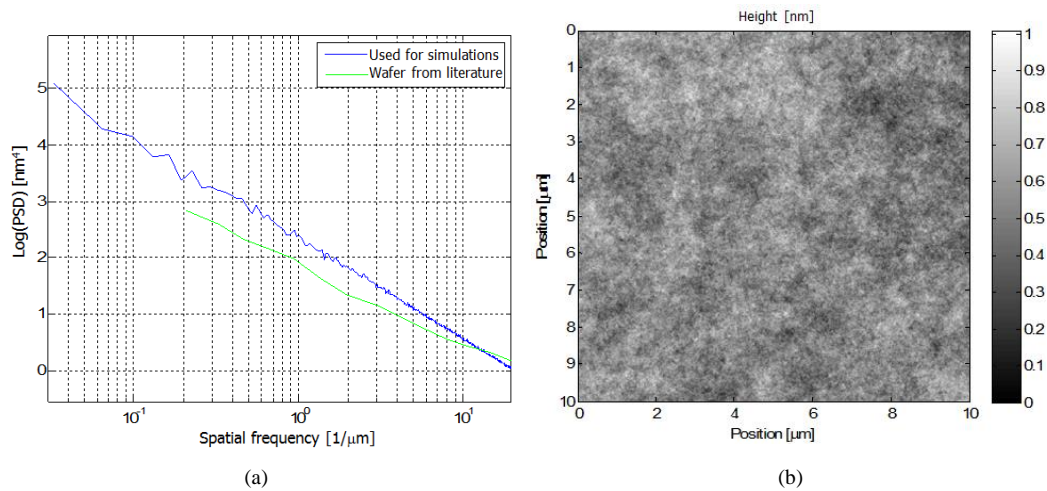
Figure 3. (a) Power spectral density of surface roughness as used throughout our simulations, and comparison to actual wafer data[9]. (b) Typical example of synthesized surface topology.

Figure 4(c) shows that the wavefront emanating from the surface (green phasors) can in fact be considered as the sum of two constituent waves: the specular reflection (red phasors) and a perturbation field due to the surface topology (blue phasors). Since the specular reflection is fully blocked by the imaging aperture, only the perturbation field will in fact contribute to image formation (Figure 4(d)).

Due to the finite (diffraction-limited) spatial resolution of the imaging system, the complex amplitude in a particular image position is the result of the coherent addition of perturbation phasors within the area corresponding to the complex point spread function. It is important to realize that the diameter of the point spread function ($\sim 1.22\lambda/NA$) will be larger than the distance over which, due to the tilt of the illumination beam, the specular (i.e. red) phasors will rotate a full cycle ($<\lambda/NA$). Since the perturbation phasors are perpendicular to the specular phasors, those too will show a mutual phase diversity of larger than 2π radians within the area encompassed by the point spread function. Consequently, as illustrated in Figure 4(e), the complex amplitude in a location of the image will be formed by the addition of phasors that have random phase and amplitude, thereby leading to a well-documented speckle pattern having random amplitude and phase. The local complex amplitude of the speckle pattern can in this case be considered the result of a two-dimensional random walk of the constituent two-dimensional phasors.

Because the speckle background negatively affects the ability to detect a particle, in the design of a particle detection system care will be taken to minimize this speckle. One possibility is to illuminate under different angles, thereby producing uncorrelated speckle backgrounds, thus averaging out the modulation in the background[1, 4]. In our comparative numerical analysis of a dark-field based detection system (see Chapter 3) we have assumed illumination under 9 different azimuths.

3. BINARY-PHASE INTERFEROMETRIC PARTICLE DETECTION

Instead of averaging out the speckle background, we aimed to improve the detection limit by using the coherent nature of the light to amplify the weakly scattered signal from the particle. Obviously, if the speckle background is amplified accordingly the signal-to-noise ratio (SNR) remains unchanged, thereby gaining nothing. We therefor aimed to develop a concept wherein the speckle background *does not* interfere with an overlapping reference beam. In Section 3.1 we will introduce an imaging concept that enables doing so, without (for now) actually adding a reference beam. In subsequent sections a reference beam will be added and the possible advantage for particle detection will be demonstrated.

3.1 Binary speckle

Since there is effectively no interference (in irradiance) between two beams that have a 90° phase shift, a first requirement for our concept is to devise an illumination and imaging scheme that results in speckle with little or no phase-diversity. A conceptual drawing of such a system is shown in Figure 5, whereas Figure 6 helps to explain the phase behavior of this system.
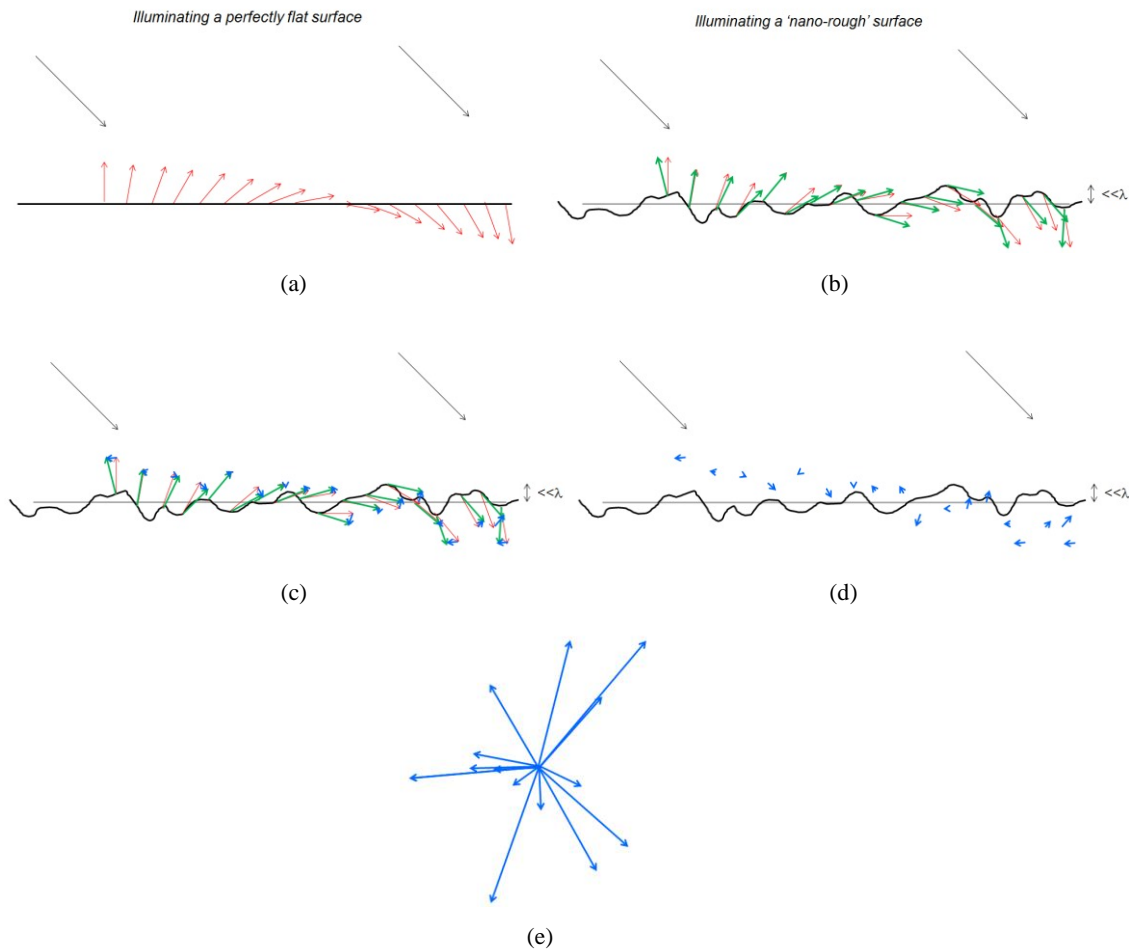

Figure 4. Illustrative explanation of the random phase behavior in the image plane of the system as shown in Figure 2. (a) A flat surface is illuminated by an off-axis beam. The red phasors represent the specularly reflected wave. In dark-field imaging this specular reflection is outside the aperture of the imaging optics. (b) A nano-rough surface is illuminated by an off-axis beam. The local surface height causes an advance or delay of the reflected wavefront (green phasors) compared to that of the specular reflection (red phasors). (c) The field from the surface (green phasors) can be considered the sum of the specular field (red phasors) and a perturbation field (blue phasors). Note that for a surface roughness much smaller than the wavelength the perturbation phasor is oriented perpendicular to the specular phasor. (d) As the specular reflection does not pass through the (dark field) optics, only the perturbation field contributes to image formation. (e) The perturbation phasors have random amplitude and phase, where the phase may take any value between 0° and 360°. Consequently, a traditional fully-developed speckle image will be formed.

Figure 5(a) shows a conceptual drawing of an on-axis illuminated annular-aperture-imaging system. Our numerical wavefront propagation simulations are based on an annular imaging numerical aperture of 0.23-0.5. Figure 5(b) shows the (peak-normalized) irradiance of the wavefront in the image plane, whereas Figure 5(c) shows its phase. In this particular illumination and imaging configuration, and for a surface roughness much smaller than the wavelength, there are only two distinct phase components present in the image. Moreover, those phase components have a ±90° phase difference with respect to the phase of the specular reflection. Figure 6 helps to explain this peculiar phase behavior.

Figure 6(a)-(d) show various components of the wavefront around the substrate, where the red, green and blue arrows again represent the local wavefront in phasor notation. Figure 6(a) shows that for an on-axis illumination beam all parts of the surface are illuminated with the same phase. It is important to realize that once again the specular reflection will not contribute to the image formation.

In full analogy with Figure 4(b), Figure 6(b) now illustrates the situation for a rough surface with the slightly advanced and delayed reflected wave component depending on local surface height. Figure 6(c) and Figure 6(d) now show that the perturbation phasors are in fact all aligned (and pointing in either direction).

Consequently, the complex wavefront in the image plane will be the addition of phasors having random amplitude but a well-defined phase (modulo 180°). As illustrated in Figure 6(e), the local complex amplitude of the speckle pattern can in this case be considered the result of a one-dimensional random walk of the constituent one-dimensional phasors (as opposed to the two-dimensional random walk of Figure 4(e)). The resulting speckle will thus have a random amplitude, but two well-defined distinct phases. We refer to this as 'binary speckle'.

In the next section we will present an interferometric particle detection system that utilizes the special properties of binary speckle.
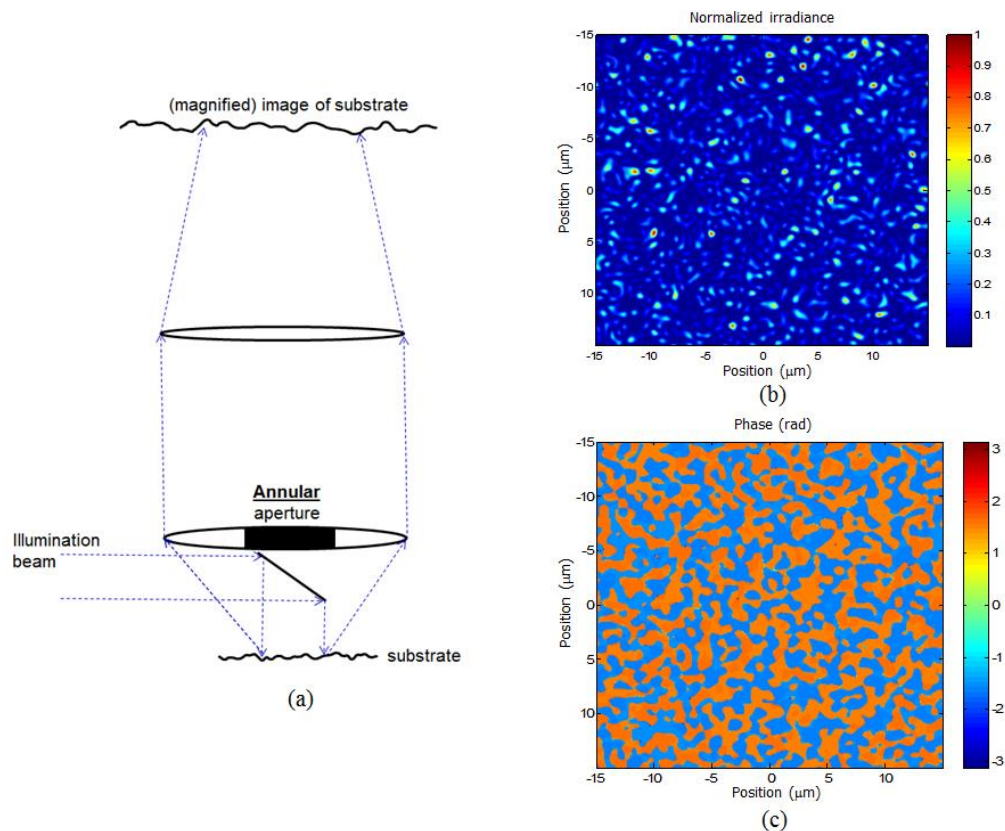

Figure 5. (a) Conceptual drawing of an on-axis illuminated annular-aperture-imaging system, (b) a typical example of the irradiance in the image plane, and (c) the phase in the image plane, where a phase of zero radians corresponds to that of the specular reflection (had it not been blocked by the aperture).
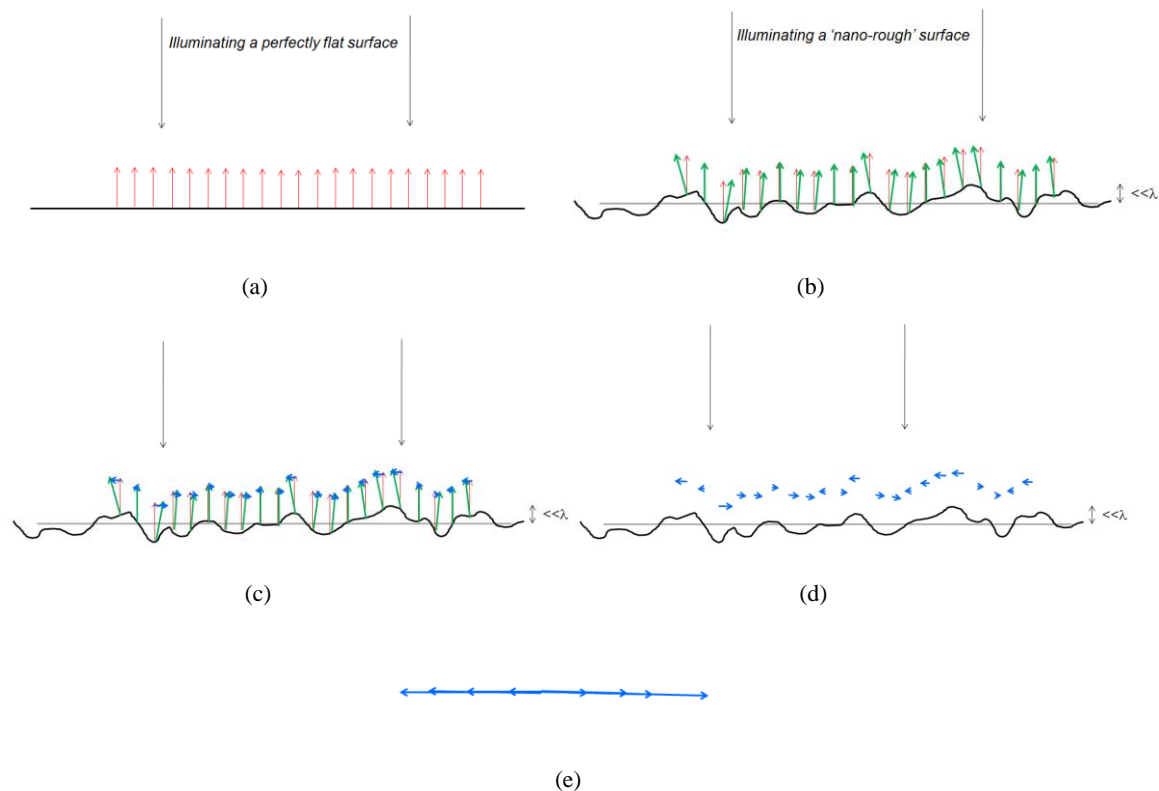
Figure 6. Illustrative explanation of the well-defined 'binary phase' behavior in the image plane of the system as shown in Figure 5. (a) A flat surface is illuminated by a beam at normal incidence. The red phasors represent the specularly reflected wave. In dark-field imaging this specular reflection is outside the aperture of the imaging optics. (b) A nano-rough surface is illuminated by a beam at normal incidence. The local surface height causes an advance or delay of the reflected wavefront (green phasors) compared to that of the specular reflection (red phasors). (c) The field from the surface (green phasors) can be considered the sum of the specular field (red phasors) and a perturbation field (blue phasors). Note that for a surface roughness much smaller than the wavelength the perturbation phasor is oriented perpendicular to the specular phasor. (d) As the specular reflection does not pass through the (dark field) optics, only the perturbation field contributes to image formation. (e) The perturbation phasors have random amplitude but show two distinct phase components. Consequently, the speckle field formed by the summation of those phasors will have a 'binary-phase'.

3.2 Interferometric particle detection

Figure 7(a) shows the system of Figure 5 but now with the addition of a reference beam. This is a possible conceptual implementation. In practice this particular implementation may be sensitive to differences in curvature (or other aberrations) between the illumination beam onto the sample and the reference beam onto the surface. Such phase deviations will cause the phase difference between the binary speckle and the reference beam to differ from 90°, resulting in undesirable coherent amplification of the speckle.

This may be solved by using the (specular reflection of) the illumination beam as the reference beam as shown conceptually in Figure 7(b). In this case illumination and reference beam will largely share the same aberrations. The Fourier filter in Figure 7(b) reduces the irradiance of the reference beam by many orders of magnitude (in order to bring the modulation of the resulting interferogram within the dynamic range of camera systems), and may adjust the phase of the reference beam if needed.
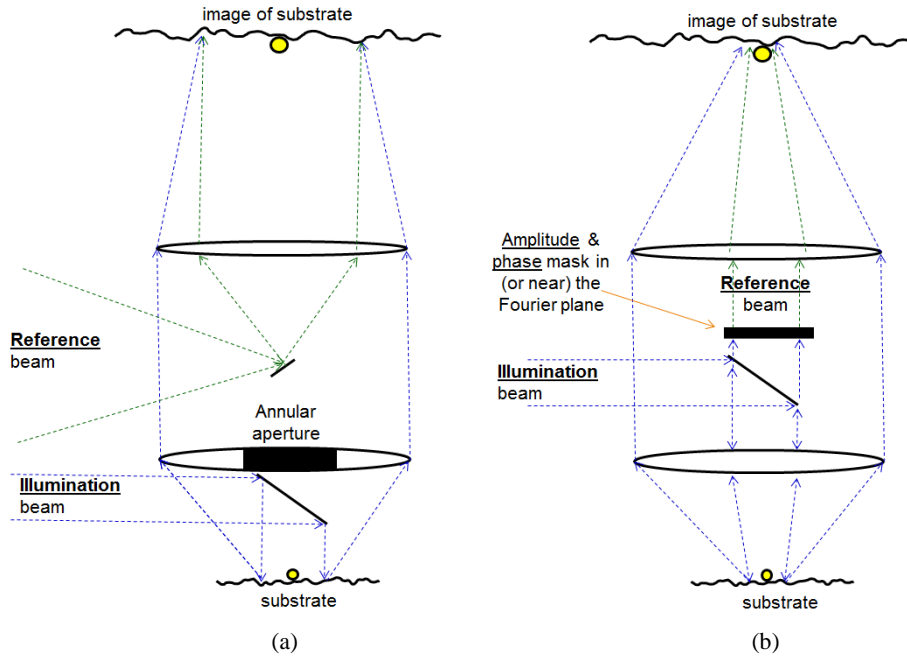
Figure 7. (a) Conceptual drawing of an interferometric particle detection system using a separately added reference beam. (b) Conceptual drawing of an interferometric particle detection system using a common-path reference beam that is created by complex amplitude filtering of the (reflected) illumination beam. The common-path system is less sensitive to aberrations of the illumination beam and is more robust with respect to vibrations.
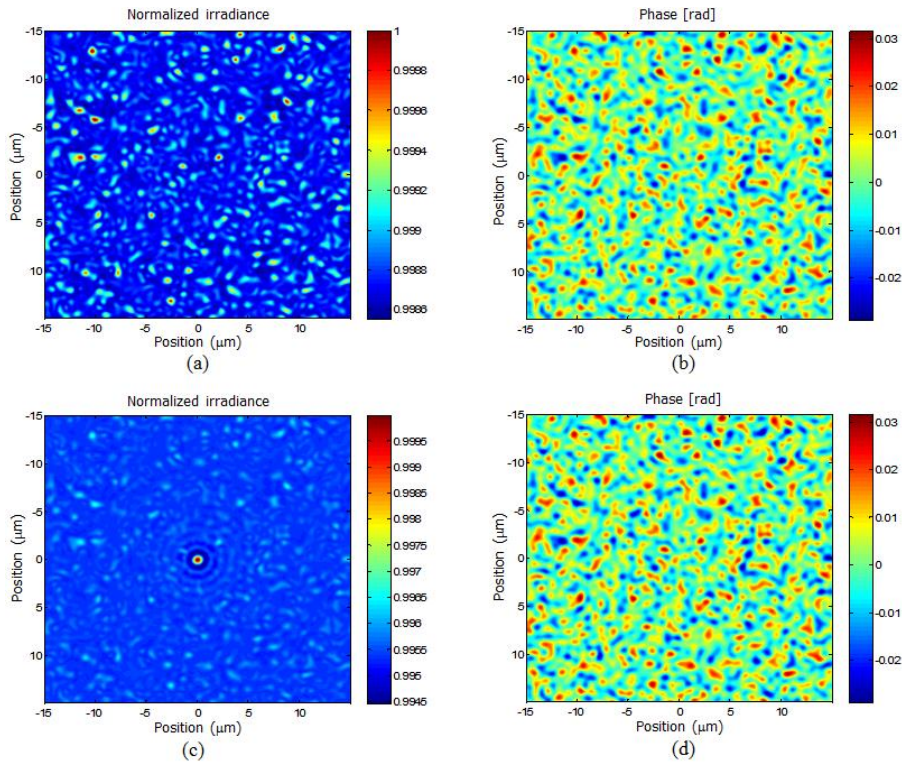

Figure 8. Irradiance and phase in the image plane without (a,b) and with (c,d) a 20 nm diameter particle on a substrate with 0.15 nm rms surface roughness.
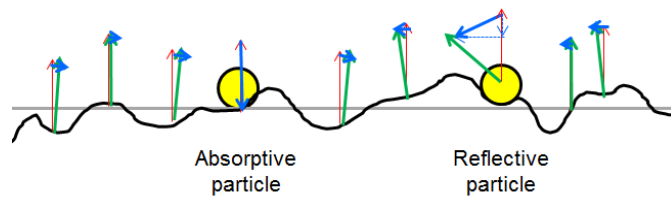
Figure 9. Illustration showing the different perturbation phasors resulting from an absorptive or reflective particle.

Figure 8 shows examples of the irradiance and phase in the image plane for the same substrate with and without a reflective 20 nm diameter particle. In the irradiance image the particle clearly stands out against the background. The particle is modelled as local topology, i.e. it has the same reflectivity, but a different height, as the surrounding substrate. Compared to absorptive particles, such reflective particles are harder to detect using our interferometric approach. Figure 9 helps to explain the difference between an absorptive (amplitude change only) and a reflective (phase change only) particle.

The perturbation field (blue phasor) due to a fully absorbing particle will have maximum amplitude and its phase will be orthogonal to that of the speckle. The resulting complex amplitude in the image will thus interfere maximally with the reference beam.

For a reflective particle (having the same reflectivity as the substrate) both the magnitude and the orientation of the perturbation phasor depend on the (effective) height of the particle. For particles much smaller than the wavelength only part of the perturbation phasor will be orthogonal to those forming the speckle. Maximal coherent amplification of the particle field is thus not possible. It being the more challenging scenario to detect, we use reflective particles throughout our analysis.

Figure 10(a) shows the peak-to-sigma ratio P as a function of particle diameter for a dark-field system as shown in Figure 2(a) and for an interferometric system as shown in Figure 7(a). The different shades of blue in Figure 10 refer to different values of the reference beam ratio (the ratio between the (mean) irradiance of the reference beam and that of the speckle background). When applying $P \geq 24$ as particle criterion, the dark-field approach allows to detect particles larger than ~22.5 nm whereas our novel interferometric approach allows to detect particles larger than 16 nm (when using a reference ratio of ~5000). The minimum detectable particle size is thus reduced by 30%, which is a tremendous gain considering that the scattered energy scales with the sixth power of the particle diameter.

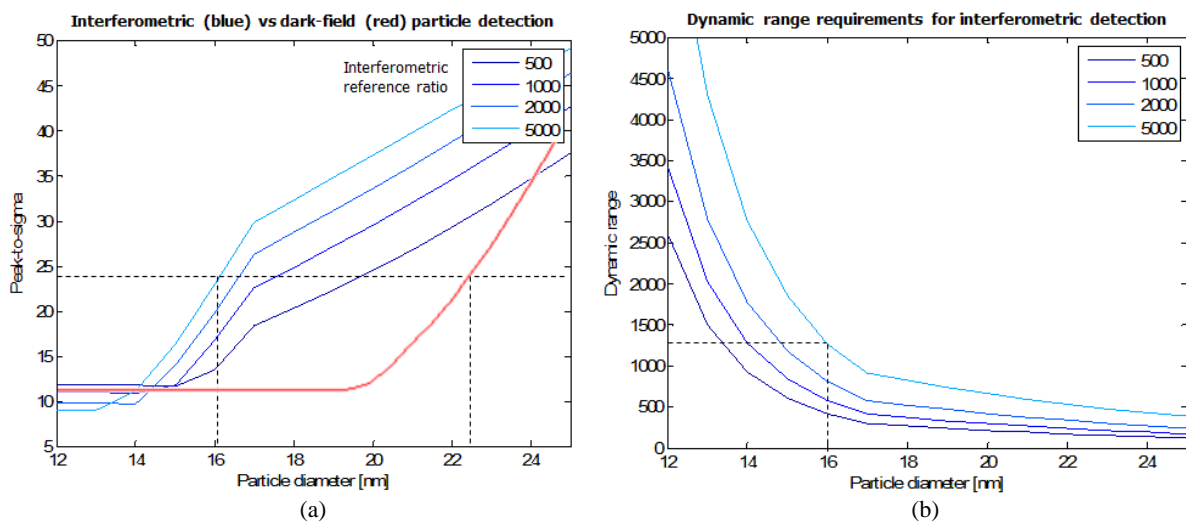(a)   (b)

Figure 10. (a) Peak-to-sigma in the image plane as a function of particle diameter for both the new interferometric approach (blue lines showing different reference ratios) and traditional approach of dark-field irradiance based detection (red line). (b) Dynamic range that is needed to record the modulation due to the particle against the mean irradiance set by the reference beam.

Figure 10(b) shows the dynamic range that is needed to capture the irradiance modulation of the particle image against that of the reference beam. Even for a reference beam ratio of 5000, i.e. needed to identify a 16 nm particle, the dynamic range can be realized with commercially available camera systems.

Using our 'binary-phase interferometric particle detection' it may be possible to reduce the particle detection limit even further. As discussed in Section 2.1 for a dark-field irradiance based system the particle image will have the same spatial appearance as a speckle. However, for our proposed interferometric system, the particle image contains a unique spatial fingerprint (as can be seen in Figure 8(c). The (diffraction limited) particle image will result in an Airy-like pattern. Since the central lobe in such an image is out-of-phase relative to the first ring around the central lobe, a distinct pattern is formed upon interference with the reference beam. If the central lobe undergoes constructive interference, the ring will undergo destructive interference, thereby leading to a pattern that is not commonly found in speckle patterns and, by applying image recognition techniques, can thus be used to obtain increased certainty in identifying a particle in an image with $P < 24$.

It is important to point out that the use of interferometric techniques for the detection of nanoparticles particles is not new[10-15]. Often however techniques deal with the detection of nanoparticles in a fluidic environment[11, 13], thereby not suffering from the surface roughness surrounding the particle. To our best knowledge, no previous study interferometrically improves the SNR of the image of nanoparticles on a (nano-)rough substrate by realizing, and deliberately exploiting, the binary phase properties of the speckle due to the surface roughness.

3.3 Aberrations

Our technique relies on distinguishing the particle light from the background light based on their phase properties. In practice the optical system used for the imaging will suffer from wavefront errors (WFE). These WFE will add phase diversity to the passing wavefronts, and will thus result in a spread of the phase around the two distinct binary components of the speckle background. The background speckle will therefor gain a field component that is in phase with, and thus will be amplified by, the reference field.

The significant impact of this effect is shown in Figure 11. Here the peak-to-sigma is calculated as a function of particle diameter for various WFE of the imaging optics. It can be seen that for increasing WFE the particle detection limit quickly deteriorates. When the WFE is ~0.3 nm the performance of the interferometric system will be comparable to that of traditional dark-field irradiance based systems. Such extreme WFE requirements lead to very complex, and thus costly, optics.
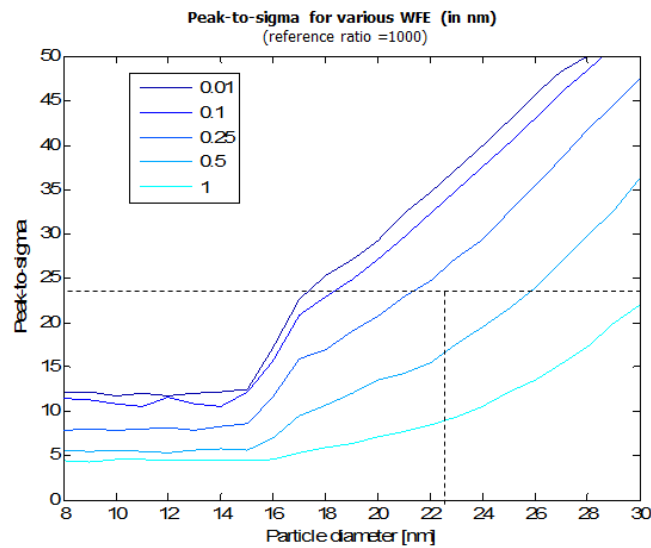

Figure 11. Peak-to-sigma as a function of particle diameter for various wavefront errors (in nm). The dashed-line refers to the detection limit of dark-field irradiance based detection.
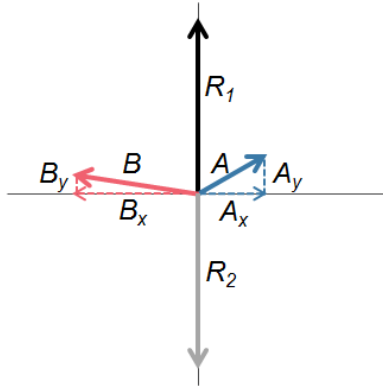
Figure 12. Phasor plot showing (*A*) light due to particle, (*B*) light due to surface scatter, and (R_1, R_2) reference beams. Interferometric amplification will work even when $A < B$, as long as $A_y > B_y$.

3.4 Irradiance modulation and dynamic range

Figure 10 shows that smaller particles can be detected when increasing the relative strength of the reference beam. Figure 12 helps to explain this behavior. In this figure the phasor R_1 represents the complex amplitude due to the (uniform) reference beam. The phasor A describes the complex amplitude due to a particle at a certain location. The phasor B represents the complex amplitude due to the speckle field at another location. Note that we have already assumed the phase of the speckle to not be perfectly binary, yielding a component B_y which will interfere with the reference beam.

At the location of A the resulting irradiance (i.e. upon interference with R_1) will be:

$$I_A = R_1^2 + A^2 + 2R_1 A_y. \tag{1}$$

Likewise, for the irradiance at the location of the speckle may be written:

$$I_B = R_1^2 + B^2 + 2R_1 B_y. \tag{2}$$

For the ratio of irradiance modulation due to a particle relative to the irradiance modulation due to speckle can thus be written:

$$M = \frac{A^2 + 2R_1 A_y}{B^2 + 2R_1 B_y}. \tag{3}$$

As discussed before, in order to differentiate a particle from the speckle background it is required that $M \gg 1$. In cases where $B > A$ (i.e. $M < 1$ for $R_1 = 0$), adding a reference beam allows to increase M to above unity as long as $A_y > B_y$.

For the limit of M (i.e. an indication for the maximum particle-to-speckle contrast that can be reached by coherent amplification of the particle light) follows:

$$M_{R_1 \to \infty} = \frac{A_y}{B_y}. \tag{4}$$

Note that Eq. (4) also helps to explain the significant impact of the aberrations (leading to an increase of B_y) that were shown in Section 3.3.

In order to detect a particle it is required that its resulting irradiance modulation $\sim 2\,R_1 A_y$ (for large values of R_1) can be measured by the sensor in the image plane. Since the signal level is largely determined by R_1^2 the dynamic range is found to be proportional to R_1 / A_y (once again showing that although increasing the reference beam strength will allow to detect smaller particles, it will impose more requirements on the dynamic range of the measurement system).

4. DIFFERENCE DETECTION

Depending on the phase and amplitude properties of the particle and speckle field, it may occur that the dynamic range requirements cannot be practically realized. In those cases 'difference detection' can be performed to further improve the detection limit.

A conceptual implementation of 'difference-detection enhanced binary-phase interferometric particle detection' is shown in Figure 13. Like the concept shown in Figure 7(b) this particular embodiment has the (stability) benefits of a common-path interferometer. The illumination beam has a linear polarization that is rotated 45°, resulting in a 50-50 split on the polarizing beam splitter. The mask in the Fourier plane is now birefringent, allowing the two orthogonal polarization components (matching those of the polarizing beam splitter) to experience a difference path length. Consequently two images of the substrate are formed, where the relative phase of the reference beam between those two images can be chosen freely. There are obviously different implementations (e.g. not involving birefringence and polarization-based splitting) that allow to obtain the phase-shifted reference beams.

The benefit of adding the extra measurement channel can be explained with the help of Figure 12. If the reference beam in the second channel is 180° phase-shifted but has an amplitude equal to that in the first channel, then for the irradiance at the location of the particle can be written:

$$I'_A = R_2^2 + A^2 - 2R_2A_y. \tag{5}$$

If the images from both measurement channels are subtracted (i.e. $I_A - I'_A$), the resulting difference image only contains a term corresponding to the interference between the reference beam and the in-phase part of the particle light:

$$I_{diff,A} = 2R_1A_y + 2R_2A_y = 4RA_y, \tag{6}$$

where $R = R_1 = R_2$.

Likewise, for the difference image due to the speckle may be written:

$$I_{diff,B} = 2R_1B_y + 2R_2B_y = 4RB_y. \tag{7}$$

From Eqs. (6) and (7) follows that for the ratio of the difference image irradiance modulation due to a particle relative to the difference image irradiance modulation due to speckle can be written:

$$M_{diff} = \frac{A_y}{B_y}. \tag{8}$$

When comparing Eq. (8) to Eqs. (3) and (4) it is found that, unlike in single-image interferometry, the particle-to-speckle ratio in a difference image is independent on the reference beam irradiance and is equal to the maximum that can be realized using single-image interferometry.

Although the value of R does not affect the contrast in the difference image, it should be chosen such that the last terms in Eqs. (1), (2) and (5) are measurable given the dynamic range of the detection system.

Figure 14 shows the simulated peak-to-sigma ratio as a function of particle diameter for the single image interferometric detection as presented in Chapter 3 (blue lines), as well as for the difference detection introduced in this chapter (orange lines). As Figure 14 shows, when using difference detection the minimum detectable particle size is indeed independent of the reference beam intensity, and is smaller than when using a single interferometric image at a reference beam ratio of 5000.

Due to the dual measurement arms the experimental setup for difference detection is more complex than that of single image binary-phase interferometric particle detection. However, since the particle-to-speckle modulation is independent of reference beam ratio, when using difference detection the requirements on the dynamic range of the detection system may be significantly lowered. Given a particular application, and depending on parameters such as particle scattering cross section and surface roughness, a trade-off should be made which implementation can best be used.

It should finally be noted that the practical performance of difference detection is also sensitive to aberrations as discussed in Section 3.3.
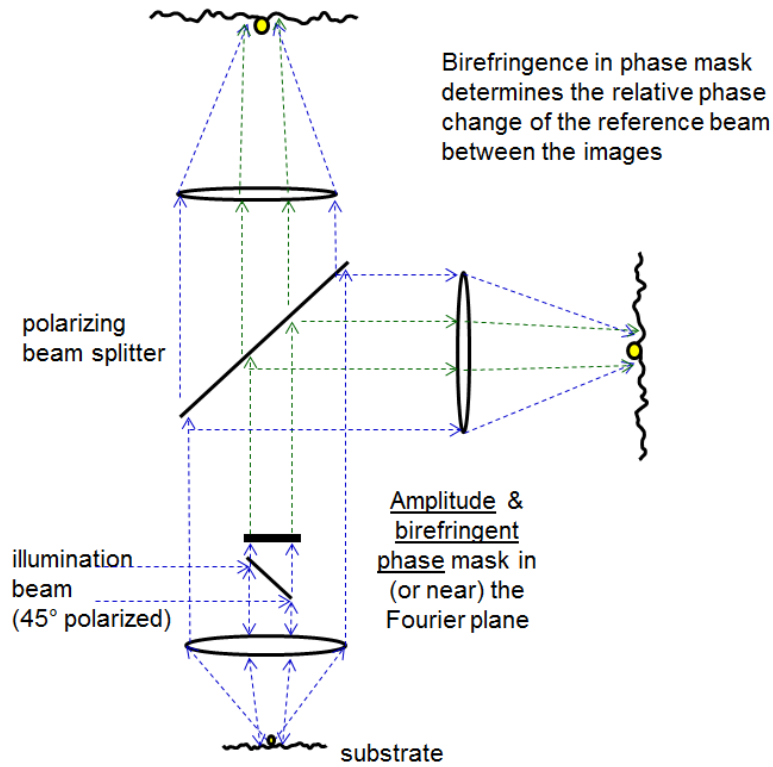
Figure 13. Conceptual schematic of a system that can be used for 'difference-detection enhanced binary-phase interferometric particle detection'. Two images of the substrate are formed, where the reference beam has a 180° relative phase-shift between both images and the phase is chosen such that no (or minimal) interference occurs between the reference beam and the light scattered due to surface roughness.
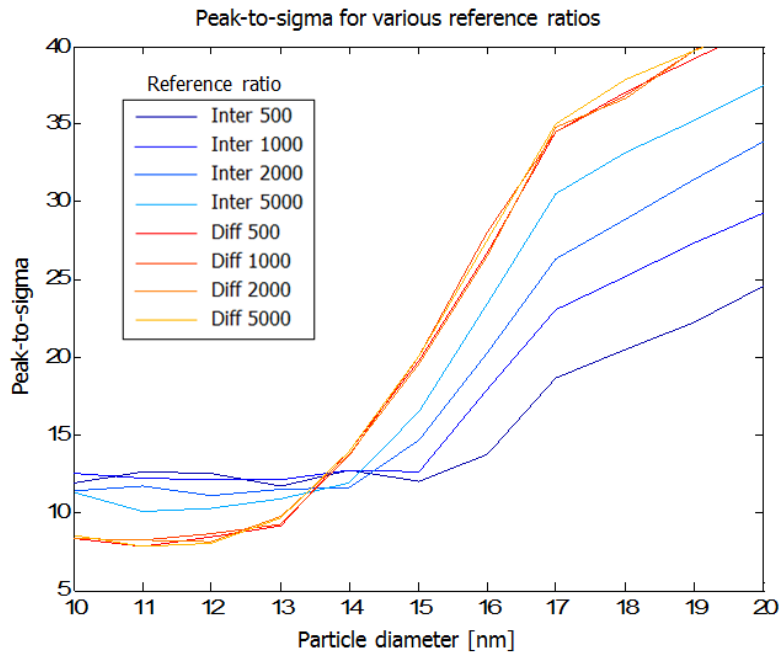

Figure 14. Peak-to-sigma of (single) interferometric images (blue lines), and of difference detection (orange lines).

5. CONCLUSION AND DISCUSSION

In this paper we have presented a new method for detecting the presence of nanoparticles on a nano-rough surface. This method, which we refer to as 'binary-phase interferometric particle detection', allows to detect much smaller particles than the state-of-the-art dark-field irradiance-based particle detection systems commonly used to inspect semiconductor wafers. Our technique is based on the realization that, when properly configuring the illumination and imaging system, the speckle image resulting from a substrate that has a sub-wavelength surface roughness may have only two distinct phase components. This allows for the coherent interferometric amplification of the weak signal due to a particle, whilst (largely) avoiding interferometric amplification of the coherent speckle background.

As the signal-to-be-detected becomes smaller relative to the (binary-)speckle background, the relative strength of the reference beam needs to be increased. This increase in reference beam strength may lead to impractical dynamic range requirements of the detection system. When using 'difference detection' these dynamic range requirements may be relaxed, at the cost of system complexity.

Our simulations show that the proposed techniques allow to robustly detect the presence of a 15-16 nm diameter particle on a substrate with 0.15 nm rms surface roughness. This is a significant improvement compared to the ~22.5 nm detection limit of a state-of-the-art dark-field irradiance based detection system.

It should be noted that all simulations assume a reflective (phase) particle, which for our technique is harder to detect than an absorbing (amplitude) particle. Potentially even smaller particles may be detectable.

The main drawback of the proposed phase-based technique is that, compared to irradiance-based techniques, it is much more sensitive to wavefront errors of the imaging optics. In fact, when the rms wavefront error of the imaging optics is larger than ~0.3 nm the interferometric approach will perform worse than traditional techniques. The practical realization of a system based on this new technique will thus require very complex, and therefor expensive, optics. There may however very well be applications where the benefits outweigh the costs.

While this paper is mainly focused on applying binary-phase interferometry, with or without difference-detection, for the detection of nanoparticles on a rough substrate, the proposed techniques are obviously more broadly applicable. These techniques may also be applied for the detection of defects such as bumps and pits, or the localization of intentionally added but weakly scattering (sub-surface) features. Finally, it is important to emphasize that the phase-nature of our technique even allows to differentiate a pit (average height below surface) from a bump (average height above surface).

REFERENCES

[1]   Walle, P. van der, Kumar, P., Hannemann S., Eijk D. van, Mulckhuyse W., Donck, J.C.J. van der, "Implementation of background scattering variance reduction on the Rapid Nano particle scanner", Proc. SPIE 9050, 33 (2014).

[2]   http://www.kla-tencor.com/Metrology/surfscan-series.html

[3]   Stokowski, S., and Vaez-Iravani, M., "Wafer inspection technology challenges for ULSI manufacturing," Proceedings of the international conference on characterization & metrology for ULSI technology 449, 405-415 (1998).

[4]   Walle, P. van der, Kumar, P., Ityaksov, D., Versluis, R., Maas, D.J., Kievit, O., Janssen, J., Donck, J.C.J. van der, "Increased particle detection sensitivity by reduction of background scatter variance", Proc. SPIE 8681, 16 (2013).

[5]   Van de Hulst, H. C., [Light scattering by small particles], Dover Publications, New York, 63-84 (1981).

[6]   Goodman, J. W., "Statistical properties of laser speckle patterns," in [Laser Speckle and Related Phenomena], 2nd ed., Dainty, J. C., Ed., Springer Verlag, New York (1984).

[7]   Dainty, J. C., "The statistics of speckle patterns," in [Progress in Optics], Wolf, E., Ed., North-Holland (1976).

[8]   Goodman, J.W., "Introduction to Fourier Optics," Roberts & Company Publishers (2005).

[9]   Duparré, A., Ferre-Borrull, J., Gliech, S., Notni, G., Steinert, J., Bennett, J., "Surface characterization techniques for determining the root-mean-square roughness and power spectral densities of optical components," Appl. Opt. 41, 154-171 (2002).

[10]   Batchelder, J. S., and Taubenblatt, M. A., U.S. Patent No. 5 037 202, (1991).

[11] Ignatovich, F.V., Novotny, L., "Real-Time and Background-Free Detection of Nanoscale Particles," Phys. rev. Lett. 96, 013901 (2006).

[12] Dijk, M. A. van, et al, "Absorption and Scattering Microscopy of Single Metal Nanoparticles," Physical Chemistry Chemical Physics, Royal Society of Chemistry, Vol. 8, pp.3486. (2006).

[13] Deutsch, B., et al, "Nanoparticle detection using dual-phase interferometry," Appl. Opt. 49 (2010)

[14] Vaez-Iravani, M., Zhao, G., U.S. Patent No. 7 295 303, (2007).

[15] Yurt, A., et al, "Widefield interferometric detection and size determination of dielectric nanoparticles ," 23rd Annual Meeting of the IEEE Photonics Society, p.197-198 (2010).